

How unique is the Asymptotic Normalisation Coefficient (ANC) method?

J.C. Fernandes*, R. Crespo†,

*Departamento de Física, Instituto Superior Técnico,
and Centro Multidisciplinar de Astrofísica (CENTRA)
Av Rovisco Pais 1096 Lisboa Codex, Portugal*

F.M. Nunes‡

*Universidade Fernando Pessoa,
Praca 9 de Abril, 4200 Porto, Portugal
and Centro Multidisciplinar de Astrofísica (CENTRA)
Av Rovisco Pais 1096 Lisboa Codex, Portugal*

(April 26, 2024)

Abstract

The asymptotic normalisation coefficients (ANC) for the vertex ${}^{10}\text{B} \rightarrow {}^9\text{Be} + \text{p}$ is deduced from a set of different proton transfer reactions at different energies. This set should ensure the peripheral character of the reaction and availability of data for the elastic channels. The problems associated with the characteristics of the data and the analysis are discussed. For a subgroup of the set of available data, the uniqueness property of the extracted ANC is fulfilled. However, more measurements are needed before a definite conclusion can be drawn.

PACS categories: 24.10.-i, 24.10.Ht, 25.40.Cm

Typeset using REVTeX

*E-mail:jcff@wotan.ist.utl.pt

†E-mail:raquel@wotan.ist.utl.pt

‡E-mail:filomena@wotan.ist.utl.pt

I. INTRODUCTION

Considerable effort, both theoretical and experimental, has been devoted in the last few years to the analysis of nuclear capture reactions. At the energies relevant for Astrophysics, (p, γ) or (α, γ) reactions have very low cross section values due to the Coulomb barrier repulsion. Thus, in many cases, the only access to the low energy region is through model dependent extrapolations of the higher energy data. In addition to this experimental limitation, many reactions of astrophysical interest involve radioactive beams which cannot be performed using conventional experimental techniques. The Coulomb dissociation [1] and the asymptotic normalisation coefficients (ANCs) extracted from transfers [2] have been put forward recently as alternative methods to obtain information about the astrophysical S-factors. As recognised by the physics community, while very appealing, these methods need to be subject to severe tests in order to assess their validity [3]. The aim of this work is to check upon the validity of the ANC method.

Given the limited sets of data for peripheral transfer reactions, the results presented here may not be conclusive. However, we hope that this work will underline the present difficulties in validating the method and motivate further measurements.

We firstly describe the ANC method (section II). Then, we analyse in detail the different reactions that will be used in the present work (section III). Particular attention will be paid to the characteristics of the data. Finally we present a discussion of the results and conclusions in section IV.

II. A SYSTEMATIC STUDY ON PROTON TRANSFER REACTIONS

The ANC method for the transfer reaction

$$A + a \rightarrow B + b \quad (a = b + x, \quad B = A + x), \quad (1)$$

relies on two assumptions. Firstly, the reaction mechanism used to describe the transfer mechanism should give direct information of the nuclear overlap integrals $\langle A|B \rangle$, $\langle a|b \rangle$. The differential cross section is given by

$$\frac{d\sigma}{d\Omega} = \frac{\mu_i \mu_f}{4\pi^2 \hbar^4} \frac{k_b}{k_a} \frac{1}{(2J_A + 1)(2J_a + 1)} \sum |T_{fi}|^2 \quad , \quad (2)$$

with μ_i , μ_f the reduced masses for the initial $(A - a)$ and final $(b - B)$ channels and k_a , k_b the incident and outgoing momenta in the centre-of-mass frame. The DWBA reaction mechanism has been used to analyse the differential cross section for the transfer reaction. The transition amplitude for the transfer reaction process in the post form is

$$T_{fi} = \sum \langle \Psi_f^{(-)} \mathcal{I}_{AB} | V_{xb} + V_{bA} - U_{bB} | \mathcal{I}_{ab} \Psi_i^{(+)} \rangle \quad . \quad (3)$$

In this equation $\Psi_f^{(-)}$ and $\Psi_i^{(+)}$ are the distorted waves in the final and initial channels respectively. \mathcal{I}_{AB} and \mathcal{I}_{ab} are the nuclear overlap integrals $\langle A|B \rangle$ and $\langle a|b \rangle$. The remnant term, $V_{bA} - U_{bB}$, (where V_{bA} is the interaction between the projectile core and the target A and U_{bB} the optical potential for the outgoing channel), is usually small and may be neglected but will be included in our calculations.

Secondly, according to the ANC method, the transfer reaction should be peripheral so that the asymptotic part of the overlap integrals gives the dominant contribution to the transition amplitude. For example, outside the range R_N of the A - x nuclear interaction, the overlap integral $\langle A|B \rangle$ becomes

$$\mathcal{I}_{AB\ell j} \approx C_{AB\ell j} W_{\eta\ell+\frac{1}{2}}(2\kappa r)/r \quad r \gg R_N \quad (4)$$

where $W_{\eta\ell+\frac{1}{2}}(2\kappa r)$ is the Whittaker function, $\eta = Z_A Z_x e^2 \mu / \kappa$ the Sommerfeld parameter, $\kappa = \sqrt{2\mu\epsilon/\hbar}$, μ and ϵ the reduced mass and the binding energy for the $(A-x)$ system. $C_{AB\ell j}$ is the the asymptotic normalisation coefficient (ANC) for the overlap function $\langle A|B \rangle$, related to the asymptotic normalisation of the single particle (s.p.) wave function $b_{AC\ell j}$ and a spectroscopic factor \mathcal{S} by [5]

$$C_{AB\ell j} = \mathcal{S}^{1/2} b_{AB\ell j} . \quad (5)$$

The ANC $C_{AB\ell j}$ defines the vertex for the virtual transitions $B \rightarrow A + x$ as shown in fig.(1). It has been shown [2,5] that as long as the reaction is peripheral, the ANC is independent of the details of the s.p. parameters used to describe the nucleus B ground state. That is, the effect of different s.p. parameters (which result in different s.p. asymptotic normalisations) is compensated by the deduced experimental spectroscopic factors such that the ANCs become independent of the s.p. model.

For proton transfer reactions, the extracted ANCs gives an alternative method of determining the zero energy cross section for the capture reaction $A + p \rightarrow B + \gamma$ or alternatively $S_{1A}(0)$ [2], providing of course that the overlap integral $\langle a|b \rangle$ is known. The spectroscopic factor is obtained (by a χ^2 fit) from the ratio between the data and the DWBA calculation in the forward angle region and defined here as \mathcal{S}_{exp} . To simplify notation we shall omit the angular momenta quantum numbers from the ANCs.

By choosing appropriate beam energies and scattering angles such that the transfer reaction remains peripheral this method is expected to provide a unique, structure model independent ANC.

The ANC method was firstly applied for extracting the S_{17} -factor from the study of the reaction ${}^7\text{Be}(\text{d},\text{n}){}^8\text{B}$ [4]. The peripheral character of the reaction and the dependence on the optical potential for the incoming and outgoing channels have been recently studied [5]. It was shown that for the DWBA analysis, the optical potentials for the entrance and outgoing channels need to be known in order to minimise uncertainties on the extracted S-factors [5,6].

The ANC method was also applied for extracting the S_{17} -factor from the study of the ${}^{10}\text{B}({}^7\text{Be},{}^8\text{B}){}^9\text{Be}$ reaction [7]. The transfer differential cross section was measured with high accuracy using an 84 MeV ${}^7\text{Be}$ radioactive beam, in the forward angle region, to ensure its peripheral character. The optical potentials for the incoming and outgoing channels were derived from folding model calculations and validated by the elastic data. From the measured transfer differential cross section the asymptotic normalisation for the virtual transitions ${}^8\text{B} \rightarrow {}^7\text{Be} + \text{p}$ and thus the $S_{17}(0)$ was extracted assuming that the ANC for the ${}^{10}\text{B} \rightarrow {}^9\text{Be} + \text{p}$ vertex was known. This ANC was determined in the same way from the analysis of ${}^9\text{Be}({}^{10}\text{B},{}^9\text{Be}){}^{10}\text{B}$ at an incident energy of 100 MeV [8].

Due to the increasing interest on this method it is timely to perform tests, to ensure its applicability. A first test of the ANC method was made in [9] where the proton transfer

reaction $^{16}\text{O}(^{3}\text{He},\text{d})^{17}\text{F}$ was analysed. It was shown in that work that the deduced S-factor for the capture reaction $^{16}\text{O}(\text{p},\gamma)^{17}\text{F}$ agreed well with the capture data. In the present work further tests are performed.

Given the ANC $C_{AB\ell j}$, the question we address here is: *how unique is this value, deduced from different proton transfer reactions or from the same reaction but at different energies, assuming that the peripheral character is satisfied?* For the present analysis we choose the case of the ANC for the $^{10}\text{B} \rightarrow ^{9}\text{Be} + \text{p}$ vertex here called C_{19} . This choice was motivated by the accurate forward angle data for the transfer reaction $^{9}\text{Be}(^{10}\text{B},^{9}\text{Be})^{10}\text{B}$, measured at a laboratory energy of 100 MeV, together with good knowledge of the optical potentials [8]. A literature search was then performed to find proton transfer data at low energy from which independent values for C_{19} could be extracted. In order to reduce the uncertainties associated with the lack of knowledge of the optical potential for the incoming and outgoing channel, our search was restricted to cases where elastic scattering data was available, whenever it was possible for both the incoming and outgoing channels. With these requirements in mind, the set of reactions used to study the uniqueness property are shown in table (I).

A spherical two-body model is used for describing the ground state of each ($\text{B} = \text{A} + \text{p}$) system. We take a Woods-Saxon potential with radius of 1.25 fm, diffuseness $a=0.65$ fm, and depth adjusted to give the appropriate binding energy ($\epsilon(\text{p} + ^9\text{B}) = 6.5858$ MeV, $\epsilon(\text{p} + ^{12}\text{C}) = 1.93435$ MeV, and $\epsilon(\text{p} + \text{d}) = 5.4935$ MeV). A spin-orbit term with the same geometry parameters and depth of 2.06 MeV was included. The ^{10}B g.s. was then described as $p_{3/2}$ proton coupled to the $^{9}\text{Be}(3/2^-)$ core ($p_{3/2} \otimes 3/2^-$), the ^{13}N g.s. as ($p_{1/2} \otimes 0^+$) and the ^3He g.s. as ($s_{1/2} \otimes 1^+$). The two-body $\text{p} - ^9\text{Be}$ s.p. model is not expected to provide a complete description for the ^{10}B system. In fact, the core ground state is close to the $\alpha\alpha n$ threshold and other terms may contribute significantly to the wave function. Within the present reaction mechanism framework, the incompleteness of the two-body model in describing the composite nucleus is taken into account through the extracted spectroscopic factor \mathcal{S}_{exp} .

In order to extract the ANC C_{19}^2 from reaction (\mathcal{A}), we proceed in the same way as in [8]. The transfer reaction (\mathcal{B}) provides similarly information on the C_{19}^2 . The $^{10}\text{B}(\text{d},^3\text{He})^9\text{Be}$ reaction (\mathcal{C}) can be expressed in terms of the product $C_{19}^2 C_{12}^2$ where C_{12} is the ANC for the vertex $^3\text{He} \rightarrow \text{d} + \text{p}$ given in [16]. As for reaction (\mathcal{D}), the DWBA cross section can be expressed in terms of the product $C_{19}^2 C_{12}^2$ where C_{12} is the ANC constant for the transition $^{13}\text{N} \rightarrow \text{p} + ^{12}\text{C}$, that was extracted from the transfer reaction (\mathcal{E}). In all cases the calculations were performed using FRESCO [10].

III. RESULTS

The experimental analysis

The elastic and transfer experimental differential cross sections, for all the reactions we are considering, are shown in figs.(2-7). For each transfer reaction, we firstly determine a set of optical potential parameters that fit the elastic channels. In doing the elastic fit we take

into account the whole angular range available. The starting parameters for this fit were taken from sets found in the literature at a nearby projectile energy. These were chosen to have considerable differences in order to truly evaluate the uncertainties on the ANCs due to the choice of optical potentials. The parameters for these optical potentials are collected in the Appendix.

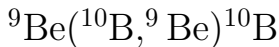
The ANC is directly related to S_{exp} (see eq.(5)). For a given pair of optical potentials (entrance and exit channels) S_{exp} is the normalisation of the forward angle DWBA cross section coming from a χ^2 fit to the transfer data. The quality of the fit (the accuracy with which the DWBA predicted angular distribution is able to reproduce the angular dependence of the data) is quantified by $\chi^2 = \frac{1}{N_{\text{exp}}} \sum_i \left(\frac{\sigma_{\text{exp}}(i) - S_{\text{exp}} \sigma_{\text{Theo}}(i)}{\Delta \sigma_{\text{exp}}(i)} \right)^2$ with N_{exp} the number of experimental points. These optical potentials are presented in tables (III-VI). To evaluate the effect of different choices of optical potentials on the calculated transfer differential cross section, we also show in these tables the corresponding χ^2 values for the transfer.

Since the aim of this method is to extract an overall normalisation of the transfer data, it is not only essential to have data with low statistical errors but, more importantly, low systematic errors. The uncertainty in the target thickness is a large contributor to the systematic error, except for the data in [8] where special attention was paid to this issue. For the (d,n) reactionm the neutron efficiency uncertainty is also quite significant. Other typical errors that may arise are due to beam collection or error in solid angle, but are much lower than those mentioned above. The systematic errors for the set of reactions are collected in table (I), according to the information in the literature. It is evident from table (I) that only the normalisation error of the data from [8] has the desired low value.

Another source of error could come from the angular range from which data is being considered. We must ensure that the peripheral character of the transfer reaction is satisfied. A large number of experimental points in the forward angle region (where the transfer is clearly peripheral) is desirable, but in most cases non-existent. For this reason, we have taken a forward angle subset of the data: the first 7 points. Even then some sets have angular ranges up to $\simeq 40^\circ$ (see table I). In two cases a smaller set of data points had to be chosen. The worst example we have considered is for the (d,n) reactions.

Finally, there will be errors on the derived ANCs arising from uncertainties on the optical potentials since the elastic data does not totally probe the interaction. The ANC errors shown in table(II) and quoted in the text are associated only with the optical potential uncertainties.

An overall panorama of the errors involved when using this method is given in fig.(8). It is clear from what has been presented in this section that our results should be interpreted as indicators until further measurements are available. They underline the need for further experimental work, before definite conclusions on the uniqueness property of the ANC method can be drawn.

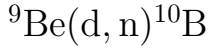


The reaction $^9\text{Be}(^{10}\text{B}, ^9\text{Be})^{10}\text{B}$ is particularly adequate for extracting the ANC since it

has the same vertex for the incoming and outgoing channels. The experimental spectroscopic factor \mathcal{S}_{exp} should then be proportional to C_{19}^4 . The elastic and transfer data at $E_{\text{lab}}=100$ MeV was taken from [8]. We take four sets of Wood-Saxon optical model potentials for the incoming elastic channel: the first two obtained by a fitting procedure to elastic data shown in fig.(2a) and the others taken from Mukhamedzhanov *et al.* [8]. For this particular reaction, the starting parameter set used in fitting the elastic data was taken from Comer [17] at 40 MeV. The fits to the elastic scattering are shown in fig.(2a). The calculated DWBA transfer cross section renormalised by the spectroscopic factor, fig.(2b), reproduces quite well the transfer data at small angles.

We note that, the calculated ANC is not strongly dependent on the details of the optical potentials pinned by the elastic data. Even if unrealistically shallow potentials are used, the ANC hardly changes. Thus, in this case, the uncertainties associated with the choice of the optical potentials are very small.

The calculated reaction cross section as a function of the partial wave, fig.(9a), clearly shows that this reaction is peripheral. In fact, the cross section at $E_{\text{lab}}=100$ MeV peaks around $L=24$ corresponding to an impact parameter of 7.29 fm which is significantly greater than the sum of the ${}^9\text{Be}$ and ${}^{10}\text{B}$ interaction radius [18,19]. For that reason the reaction cross section only becomes significantly smaller for a cutoff radius much bigger than the interaction radius. We obtained for the ANC, $\underline{C_{19}^2 = 4.9 \pm 0.25 \text{ fm}^{-1}}$, where, as mentioned before, the error is associated with an optical potential uncertainty. This is in good agreement with the value obtained in [8].

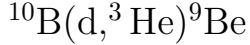


The reaction ${}^9\text{Be}(\text{d}, \text{n}){}^{10}\text{B}$ provides direct information on the C_{19}^2 as the vertex for the deuteron is well known. We performed calculations for 2 different deuteron laboratory energies: 7 and 15 MeV.

At 7 MeV we used transfer data from Park [11] and elastic data for ${}^9\text{Be}(\text{d}, \text{d})$ at 6.3 MeV from Djalois [20]. For the incoming channel, optical model potential parameters were obtained from fitting the data shown in fig.(3 a). For the outgoing channel, the potential parameters were taken from Dave and Gould [21]. As follows from the fig.(3 b), the calculated transfer differential cross section describes quite well the data. We extracted an ANC of $\underline{C_{19}^2 = 4.8 \pm 0.35 \text{ fm}^{-1}}$ which is in good agreement with our previous result obtained from the analysis of reaction \mathcal{A} .

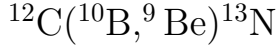
At 15 MeV we also used transfer data from Park [11] and elastic ${}^9\text{Be}(\text{d}, \text{d})$ at 15 MeV from Armstrong [22] published by [11]. Four entrance potential parameter sets were obtained fitting the data. The outgoing parameter set was taken from [21] at the appropriate energy. As can be seen from fig.(3 c), and fig.(3 d) the 4 parameter sets used describe quite well the elastic data, but none is able to reproduce satisfactorily the transfer data in the low angle region ($\theta \leq 20^\circ$). As a result, the calculated ANCs depend crucially on both the input parameter set type, surface or volume (about 20 %), and on the low angle region chosen to minimise χ^2 in order to obtain \mathcal{S}_{exp} (*vide* table(II)). The derived value for the ANC at this energy is $\underline{C_{19}^2 = 6.09 \pm 0.54 \text{ fm}^{-1}}$ which is higher than that found by [8]. As can be

concluded from fig.(11a) and fig.(11c), while the reaction is peripheral at 7 MeV, this is no longer the case for 15 MeV. Thus, this data is not useful for the purpose of this work.



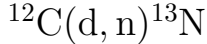
The proton pickup reaction $^{10}\text{B}(\text{d}, ^3\text{He}) ^9\text{Be}$ has two different vertices, $^{10}\text{B} \rightarrow ^9\text{Be} + \text{p}$ and $^3\text{He} \rightarrow \text{d} + \text{p}$, and therefore the experimental spectroscopic factor will be proportional to the ANCs product $C_{19}^2 C_{12}^2 = \mathcal{S}_{\text{exp}} b_{19}^2 b_{12}^2$.

The transfer and elastic data for this reaction at $E_{\text{lab}}=11.8$ MeV was taken from [12]. For the entrance channel, one parameter set was obtained fitting the elastic data shown in fig.(4a). For the exit channel, we used three parameter sets from literature: the first from [12], the second from [24] and the third from [11]. The description of transfer data shown in fig.(4b) is very reasonable, specially for the low angle region. The analysis of the reaction cross section as a function of the partial wave number shows that this transfer reaction is peripheral fig.(9b). By renormalising the calculated DWBA differential cross section from the data we obtained $C_{19}^2 C_{12}^2 = 19.17 \pm 1.82 \text{ fm}^{-2}$. For the $^3\text{He} \rightarrow \text{d} + \text{p}$ vertex, we used the value taken from [16] $C_{12}^2 = 3.9 \pm 0.06 \text{ fm}^{-1}$. Consequently, we get $\underline{C_{19}^2 = 4.92 \pm 0.54 \text{ fm}^{-1}}$, in good agreement with the result of [8].



We proceed in our systematics by looking at other proton stripping reactions involving ^9Be . A candidate for which measured data was found is $^{12}\text{C}(\text{d}, ^9\text{Be}) ^{13}\text{N}$ at 100 MeV [13]. The elastic scattering fig.(5a) was taken from [13]. We also take the same data for the outgoing channel due to the absence of experimental measurements for this channel. When fitting the elastic data for the incoming channel, we obtain four parameter sets. The optical potential parameters for the outgoing elastic channel were taken to be the same but with an appropriate radius as discussed in the Appendix. The calculated DWBA cross section describes quite well the transfer data shown in fig.(5b) specially for sets 2, 3 and 4.

As this reaction has two different vertices for the two composite nuclei, $^{10}\text{B} \rightarrow ^9\text{Be} + \text{p}$ and $^{13}\text{N} \rightarrow ^{12}\text{C} + \text{p}$, the experimental spectroscopic factor \mathcal{S}_{exp} will be proportional to the ANCs product, $C_{19}^2 C_{12}^2 = \mathcal{S}_{\text{exp}} b_{19}^2 b_{12}^2$. We obtained $C_{19}^2 C_{12}^2 = 7.4 \pm 0.5 \text{ fm}^{-2}$.



In order to extract C_{19}^2 from the results obtained with the last reaction, it is necessary to extract C_{12}^2 from another independent reaction. We chose the $^{12}\text{C}(\text{d}, \text{n}) ^{13}\text{N}$ reaction at two different energies: 9 and 12.4 MeV.

At 9 MeV we used transfer data available from two different sources, Davis *et al.* [14]

and Schelin *et al.* [15]. We take 3 sets of potential parameters from fitting the entrance channel elastic data of [27] shown in fig.(6a), and one set for the exit channel data of [21] for $^{13}\text{C}(\text{n},\text{n})$ at 10 MeV shown in fig.(6b). As shown in fig.(6c) the shape of the calculated DWBA differential cross section adjusts much better to Davis's data than to Schelin's in the low angle region, $\theta \leq 35^\circ$. Not surprisingly the derived spectroscopic factors from the two data sets differ by 30 %. We found $C_{1\ 12}^2 = 2.56 \pm 0.37$ for [15] and $C_{1\ 12}^2 = 3.31 \pm 0.45$ for [14]. Again, these errors are associated only with the optical potential uncertainty. Using the results for the ANC product from reaction $^{12}\text{C}(\text{B}^{10}, \text{Be}^9)^{13}\text{N}$ we obtain respectively $C_{19}^2 = 2.98 \pm 0.63 \text{ fm}^{-1}$ and $C_{19}^2 = 2.30 \pm 0.47 \text{ fm}^{-1}$.

An energy average differential cross section data, at 12.4 MeV, is given in Schelin's work [15] (using 13.0 MeV data and 11.8 MeV data of Mutchler [25]). For the entrance channel we used the Matusevich [26] experimental points at 13.6 MeV fig.(7a). The exit channel data was taken from [21] for $^{13}\text{C}(\text{n},\text{n})$ at 12 MeV fig.(7b). Three parameter set fits were obtained for the deuteron potential and one for the neutron potential.

As follows from fig.(7c), a good agreement in the low angle region ($\theta \leq 40^\circ$) is achieved between the data and the calculated cross section. The calculated spectroscopic factors lead us to $C_{1\ 12}^2 = 1.65 \pm 0.2 \text{ fm}^{-1}$. Using the ANC product from the reaction for $^{12}\text{C}(\text{B}^{10}, \text{Be}^9)^{13}\text{N}$, one obtains $C_{19}^2 = 4.6 \pm 0.9 \text{ fm}^{-1}$.

We note from figures (11b) and (11d) that while the reaction $^{12}\text{C}(\text{d},\text{n})^{13}\text{N}$ is peripheral at 9 MeV, the situation is rather unclear at 12.4 MeV. Although the impact parameter is greater than the ^{12}C interaction radius [18], the reaction cross section drops significantly for a cutoff radius $R_{\text{cut}} = 1 \text{ fm}$.

The experimental situation concerning this reaction is rather unsatisfactory due to different available data at 9 MeV. In the works of Davis [14] and Shelin [15], a contribution due to compound nucleus formation to the cross section is estimated using the Hauser-Feshbach statistical model. For the $^{12}\text{C}(\text{d},\text{n})^{13}\text{N}$ reaction at 12.4 MeV, the calculated compound nucleus cross section lead to an overestimation of the cross section at large angles. The Hauser-Feshbach model is then clearly inadequate in this case. Arbitrary reduction factors can be found in [14,15] producing a large uncertainty on the derived spectroscopic factors and ANCs. In order to extract a meaningful ANC factor from a transfer reaction, the reaction mechanism should be properly understood.

Since no information on the uncertainty of the absolute cross section for reaction \mathcal{D} is given [13] the C_{19} thus extracted should not be used to validate the ANC method. Agrivating the situation are the differences between the $^{12}\text{C}(\text{d},\text{n})$ data sets suggesting that the $C_{1\ 12}$ are not sufficiently reliable to be taken into account.

IV. CONCLUSIONS

We have determined the ANC for the $^{10}\text{B} \rightarrow \text{Be}^9 + \text{p}$ using a set of proton-transfer reactions at different energies. The calculated ANCs from the different reactions reproduced in fig.(8) clearly reveals the present experimental situation if one wants to check the validity of the ANC method. The sum of the contributions of the statistical, optical potential and systematic uncertainties is in most cases quite large. The graph evidently shows that, from a particular set of transfer reactions (those that are clearly peripheral and have quotable

normalisation errors), the uniqueness property of the ANC is satisfied. However, with the present data, we cannot undoubtedly conclude if this property is fulfilled.

More data for both, the transfer and elastic channels, with good resolution and carefully normalised cross sections in the forward angular region, is **crucial** if we want to unambiguously check the uniqueness of the ANCs. The elastic data is essential to reduce the optical parameter uncertainties. In the measurements special attention should be paid to minimise the uncertainty on the target thickness. For (d,n) reaction it is important to reduce as much as possible the neutron efficiency error, given that this may be a large source of uncertainty.

Even though the DWBA method is widely used, care should be taken to fully understand the reaction mechanisms before extracting the ANCs. Early studies on the deuteron breakup effects on the differential cross section indicate [28] that DWBA analysis may not be a useful tool to study deuteron transfer reactions. However, even nowadays, these reactions are still used to extract ANCs [4]. More data on deuteron transfer reactions is necessary in order to have a better understanding of the mechanisms and to check if they can be used to extract the ANCs. Generally, further tests on the ANC method, focusing on the reaction mechanism, should also be performed.

ACKNOWLEDGMENTS

This work was supported by Fundação de Ciência e Tecnologia (Portugal) through grant Praxis PCEX/C/FIS/4/96. We would like to thank L. Trache for providing us with the experimental results for the ${}^9\text{Be}({}^{10}\text{B}, {}^9\text{Be}){}^{10}\text{B}$ reaction and elastic data.

APPENDIX

We collect in tables (III-VI) the optical potential parameters obtained by fitting the elastic channels. The potentials are calculated using the following expressions:

$$\begin{aligned}
 \text{Real central : } U_R &= -V \frac{f(r)}{1+f(r)} , \\
 \text{Imaginary central volume : } U_I &= -W \frac{f(r)}{1+f(r)} , \\
 \text{Imaginary central surface : } U_W &= -4W_d \frac{f(r)}{(1+f(r))^2} , \\
 \text{Spin - Orbit : } U_{SO} &= -\frac{4}{ra_{SO}} V_{SO} \frac{f(r)}{(1+f(r))^2} \vec{l} \cdot \vec{s} , \tag{6}
 \end{aligned}$$

with $f(r) = e^{-\frac{r-R}{a_i}}$ and $R = r_i A_T^{1/3}$ except the $^{12}\text{C}(^{10}\text{B}, ^9\text{Be})^{13}\text{N}$ case where $R = r_i(A_P^{1/3} + A_T^{1/3})$. For all set of optical potentials, we use $r_i = r_0$ for real central, etc.

REFERENCES

- [1] T. Motobayashi *et al.*, Phys. Rev. Lett. **73** (1994) 2027.
- [2] H.M. Xu, C.A. Gagliardi, R.E. Tribble, A.M. Mukhamedzhanov and N.K. Timofeyuk, Phys. Rev. Lett. **73** (1994) 2027
- [3] E.G. Adelberger *et al.*, Rev. Mod. Phys. **70** (1998) 1265.
- [4] W. Liu *et al.*, Phys. Rev. Lett. **77** (1996) 611.
- [5] J.C. Fernandes, R. Crespo, F.M. Nunes and I.J. Thompson Phys. Rev. **C59** (1999) 2856.
- [6] C.A. Gagliardi *et al.*, Phys. Rev. Letts. **80** (1998) 421.
- [7] A. Azhari *et al.*, Phys. Rev. Lett. **82** (1999) 3960.
- [8] A.M. Mukhamedzhanov, *et al.*, Phys. Rev. **C56** (1997) 1302.
- [9] C.A. Gagliardi *et al.*, Phys. Rev. **C59** (1999) 1149.
- [10] I.J. Thompson, Comp. Phys. Rep., **7** (1988) 167.
- [11] J. T. Park *et al.*, Nucl. Phys. **A134** (1969) 277.
- [12] W. Fitz *et al.*, Nuc. Phys. **A101** (1967) 449.
- [13] K.G. Nair *et al.*, Phys. Rev. Lett. **33** (1974) 1588.
- [14] J.R. Davis and G.U. Din, Nucl. Phys. **A179** (1972) 101.
- [15] H.R. Schelin *et al.*, Nucl. Phys. **A414** (1984) 67.
- [16] A. M. Mukhamedzhanov *et al.*, Phy. Rev. **C51** (1995) 3472.
- [17] L.M. Comer *et al.*, Phys. Rev. **C45** (1992) 1803.
- [18] R.B Barret and D.F. Jackson, *Nuclear Sizes and Structures*, Claredon Press, (1979).
- [19] I. Tanihata *et al.*, Phys. Lett. **B160** (1985) 380; *ibid* **B206** (1988) 592.
- [20] A. Djalois *et al.*, Nucl. Phys. **A163** (1971) 131.
- [21] J.H. Dave and C.R. Gould, Phys. Rev. **C28** (1983) 2212.
- [22] D.D. Armstrong *et al.*, Los Alamos Scient. Lab. Report LA-4177, (1969) (unpublished).
- [23] Yong Sook Park *et al.*, Phys. Rev. **C8** (1973) 1557.
- [24] M. A. Crosby *et al.*, Nucl. Phys. **A95** (1967) 639.
- [25] G.S. Mutchler *et al.*, Nucl. Phys. **A172** (1971) 469.
- [26] V.A. Matusevich *et al.*, Sov. Jour. Nucl. Phys. **15** (1972) 375.
- [27] Michikatsu Takai *et al.*, Jour. Phys. Soc. Jap. **43** (1977) 17.
- [28] N. Austern, Y. Iseri, M. Kamimura, M. Kawai, G. Rawitscher and M. Yahiro, Phys. Rep. **154** (1987) 125.

TABLES

TABLE I. Set of reactions used in our analysis.

A(a,b)B	E (MeV)	l Label	Ref.	Sys. Error	N _{exp}	θ _{min}	θ _{max}
⁹ Be(¹⁰ B, ⁹ Be) ¹⁰ B	100	\mathcal{A}	[8]	7 %	7	0.5°	6.5°
⁹ Be(d, n) ¹⁰ B	7	\mathcal{B}	[11]	20 %	7	5.7°	40.°
	15		[11]	20 %	7	10.9°	44.3°
¹⁰ B(d, ³ He) ⁹ Be	11.8	\mathcal{C}	[12]	25 %	3	19.2°	31.5°
¹² C(¹⁰ B, ⁹ B) ¹³ N	100	\mathcal{D}	[13]	-	7	14.2°	27.0°
¹² C(d, n) ¹³ N	9	\mathcal{E}	[15]	12 %	6	10.8°	36.9°
	9		[14]	16 %	7	0.7°	27.1°
	12.4		[15]	20 %	4	18.0°	33.2°

TABLE II. Deduced ANC factors for $^{10}\text{B} \rightarrow ^9\text{Be} + \text{p}$. The quoted uncertainties arise from optical model analysis of the elastic channels.

A(a,b)B	E (MeV)	$\overline{S_{exp}}$	$\overline{\chi^2}$	$\overline{C_{19}^2}$ (fm ⁻¹)
⁹ Be(¹⁰ B, ⁹ Be) ¹⁰ B	100	0.52	0.80	4.90 ± 0.25
⁹ Be(d, n) ¹⁰ B	7	0.42	4.29	4.80 ± 0.35
¹⁰ B(d, ³ He) ⁹ Be	11.8	0.48	4.07	4.92 ± 0.54

TABLE III. Optical potential parameters for the $^{10}\text{B} + ^{12}\text{C}$ elastic scattering at 100 MeV.

Set	V (MeV)	r_0 (fm)	a (fm)	W (MeV)	r_w (fm)	a_w (fm)	r_c (fm)	χ^2
FIT1	27.62	1.105	0.802	17.17	1.179	0.531	1.03	2.18
FIT2	129.3	0.652	0.968	25.76	0.944	0.822	1.03	1.12
FIT3	215.2	0.548	0.956	30.41	0.900	0.841	1.03	1.29
FIT4	200.9	0.588	0.935	31.02	0.944	0.768	1.03	1.80

TABLE IV. Optical potential parameters for the ${}^3\text{He} + {}^9\text{Be}$ elastic scattering at 11.8 MeV.

Set	V (MeV)	r_0 (fm)	a (fm)	W (MeV)	r_w (fm)	a_w (fm)	W_d (MeV)	r_d (fm)	a_d (fm)	V_{SO} (MeV)	r_{SO} (fm)	a_{SO} (fm)	r_c (fm)	χ^2
T1 [12]	149.3	1.100	0.733				7.650	1.980	0.700	5.000	1.100	0.733	1.40	5.98
T2 [24]	109.0	1.600	0.640	22.00	1.600	0.640							1.30	3.51
T3 [11]	171.0	1.200	0.510				18.00	1.200	1.990	5.500	1.200	0.510	1.30	2.71

TABLE V. Optical potential parameters for d + A elastic scattering.

A (MeV)	E (MeV)	Set	V (MeV)	r_0 (fm)	a (fm)	W (MeV)	r_w (fm)	a_w (fm)	W_d (MeV)	r_d (fm)	a_d (fm)	V_{SO} (MeV)	r_{SO} (fm)	a_{SO} (fm)	r_c (fm)	χ^2
${}^9\text{Be}$	7	FIT1	130.0	1.043	0.768				78.05	1.681	0.166	7.498	1.956	0.184	1.30	4.28
${}^9\text{Be}$	15	FIT1	58.49	1.321	0.781				9.278	1.711	0.670	1.297	1.063	0.473	1.30	2.91
${}^9\text{Be}$	15	FIT2	82.45	1.015	0.986	34.51	1.145	0.867				0.922	1.040	1.104	1.25	8.35
${}^9\text{Be}$	15	FIT3	90.53	0.841	1.019	39.36	0.669	1.060				0.787	0.687	0.920	1.25	4.90
${}^9\text{Be}$	15	FIT4	95.67	1.655	0.551				46.99	1.457	0.300	3.293	1.294	2.442	1.25	11.8
${}^{10}\text{B}$	11.8	FIT1	80.55	0.924	0.972	28.89	0.853	0.732				5.066	0.760	0.879	1.30	
${}^{12}\text{C}$	9	FIT1	130.9	0.894	0.963				9.468	2.066	0.381	4.302	1.512	0.184	1.30	0.19
${}^{12}\text{C}$	9	FIT2	127.8	0.941	0.940				8.851	2.028	0.397	4.393	1.459	0.246	1.30	0.18
${}^{12}\text{C}$	9	FIT3	121.6	0.925	0.968				10.74	1.854	0.405	7.525	1.993	0.497	1.30	0.08
${}^{12}\text{C}$	12.4	FIT1	121.4	0.891	0.872				10.20	1.856	0.517	2.720	0.971	1.344	1.30	3.44
${}^{12}\text{C}$	12.4	FIT2	111.8	0.965	0.812				8.405	1.859	0.582	2.870	0.638	1.072	1.30	3.38
${}^{12}\text{C}$	12.4	FIT3	118.5	0.864	1.023				11.77	1.677	0.503	4.880	1.943	0.439	1.30	4.72

TABLE VI. Optical potential parameters for n + A elastic scattering.

A (MeV)	E (MeV)	Set	V (MeV)	r_0 (fm)	a (fm)	W_d (MeV)	r_d (fm)	a_d (fm)	V_{SO} (MeV)	r_{SO} (fm)	a_{SO} (fm)
${}^{10}\text{B}$	7	DG [21]	44.45	1.387	0.464	8.757	1.336	0.278	5.500	1.150	0.500
${}^{10}\text{B}$	15	DG [21]	42.16	1.387	0.464	14.12	1.336	0.278	5.500	1.150	0.500
${}^{13}\text{N}$	9	FIT1	68.05	0.968	0.446	18.53	1.445	0.101	7.073	0.631	0.194
${}^{13}\text{N}$	12.4	FIT1	50.50	1.203	0.329	3.902	0.400	0.867	7.096	1.444	0.353

FIGURES

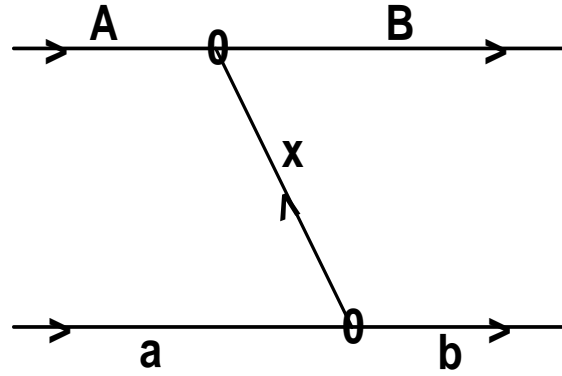


FIG. 1. Vertex diagram for the transfer reaction $A(a,b)B$.

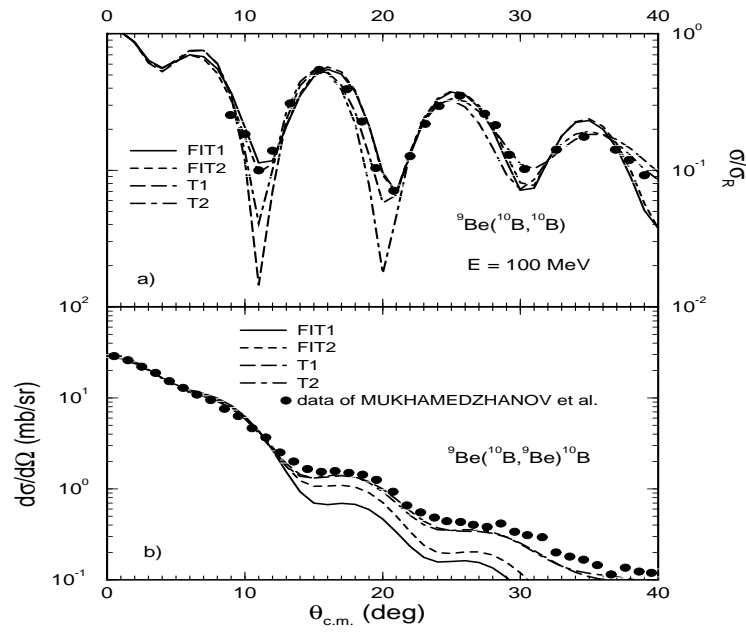


FIG. 2. Incoming elastic and transfer differential cross section for ${}^9\text{Be}({}^{10}\text{B}, {}^9\text{Be}){}^{10}\text{B}$ at $E_{\text{lab}} = 100$ MeV.

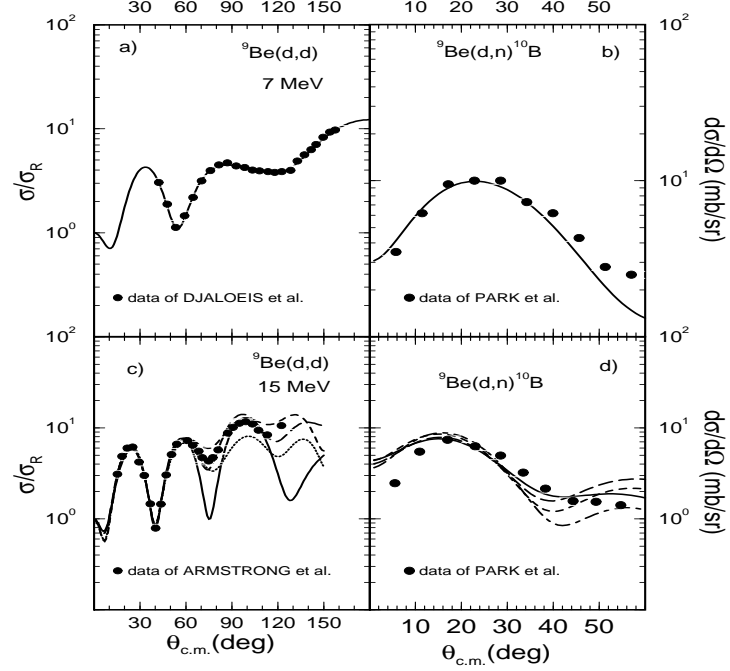


FIG. 3. Incoming elastic and transfer differential cross sections for ${}^9\text{Be}(\text{d},\text{n}){}^{10}\text{B}$ at $E_{\text{lab}} = 7$ and 15 MeV.

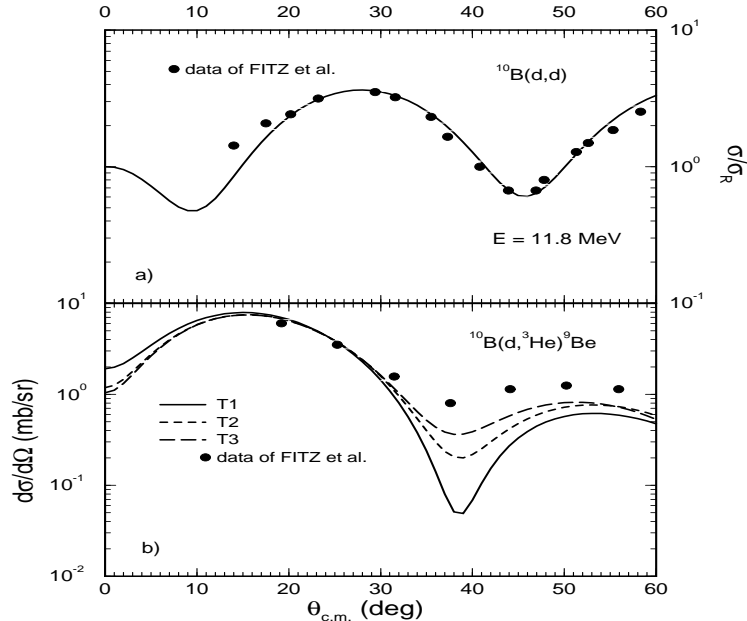


FIG. 4. Incoming elastic and transfer differential cross sections for ${}^{10}\text{B}(\text{d},{}^3\text{He}){}^9\text{Be}$ at $E_{\text{lab}} = 11.8$ MeV.

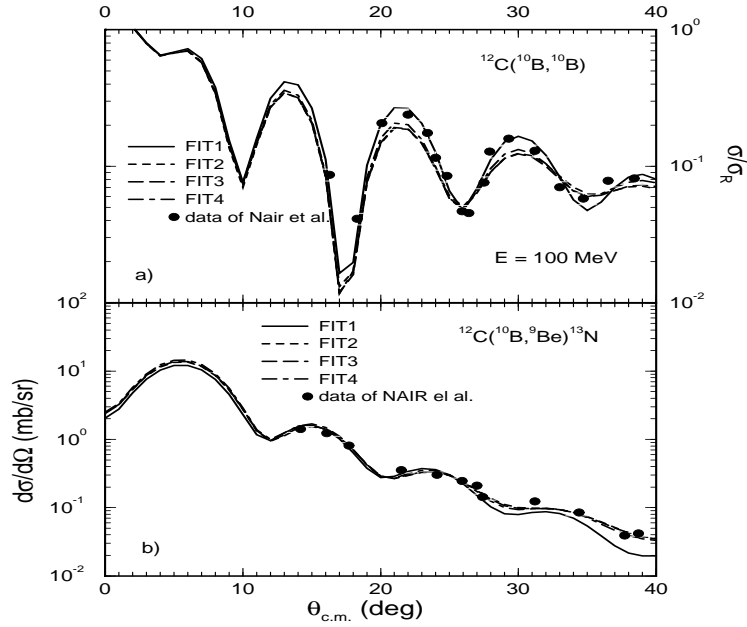


FIG. 5. Incoming elastic and transfer differential cross sections for $^{12}\text{C}(^{10}\text{B}, ^9\text{Be})^{13}\text{N}$ at $E_{\text{lab}} = 100$ MeV.

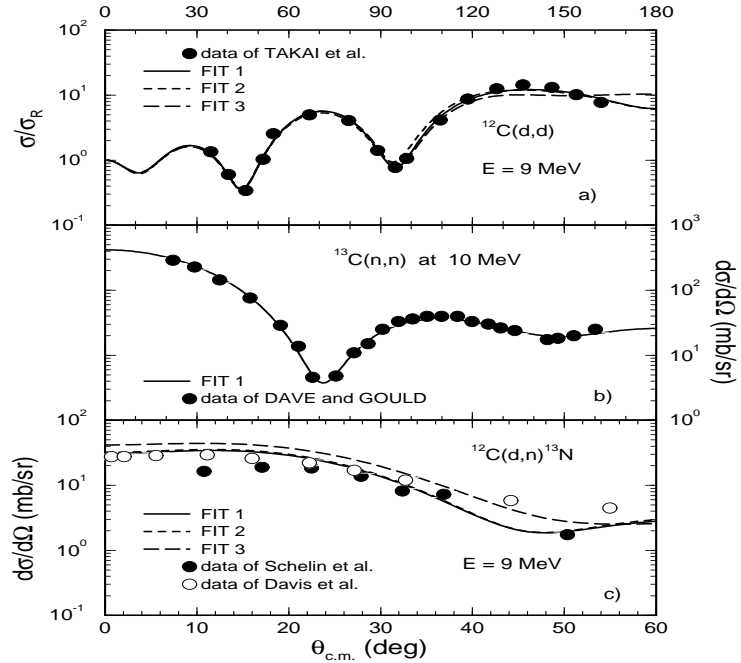


FIG. 6. Incoming elastic and transfer differential cross sections for $^{12}\text{C}(\text{d},\text{n})^{13}\text{N}$ at $E_{\text{lab}} = 9$ MeV.

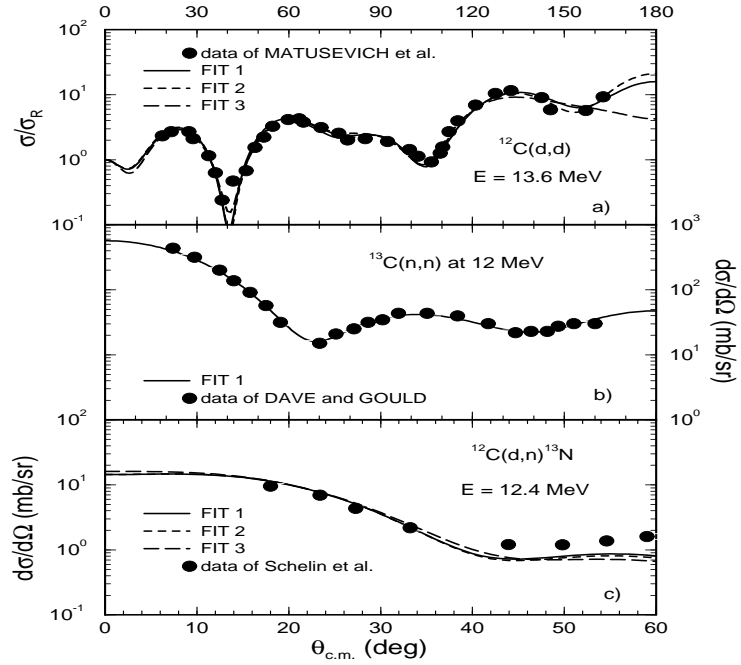


FIG. 7. Incoming elastic and transfer differential cross sections for $^{12}\text{C}(\text{d},\text{n})^{13}\text{N}$ at $E_{\text{lab}} = 12.4$ MeV.

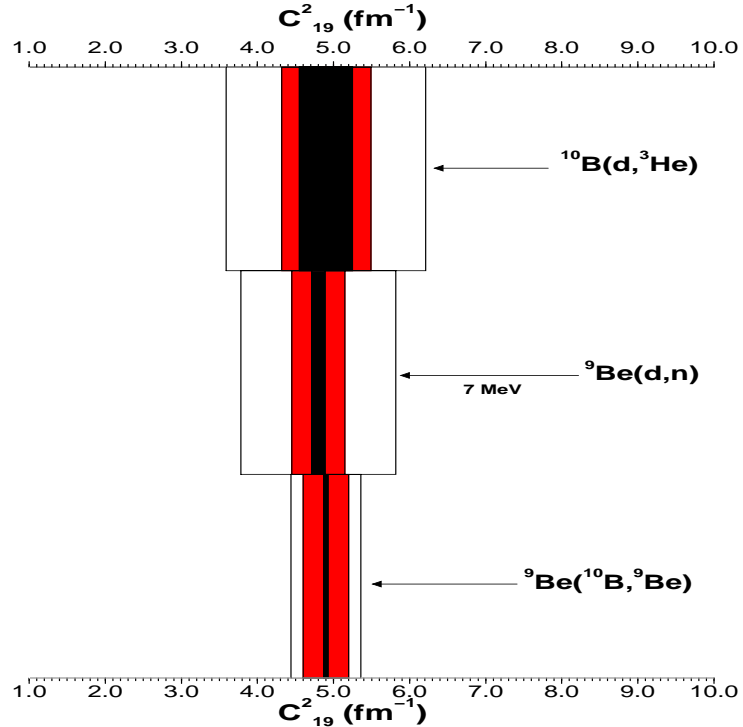


FIG. 8. Sum of the contributions of the statistical (dark bar), optical potential (light grey bar) and systematic (white bar) uncertainties for the calculated ANCs.

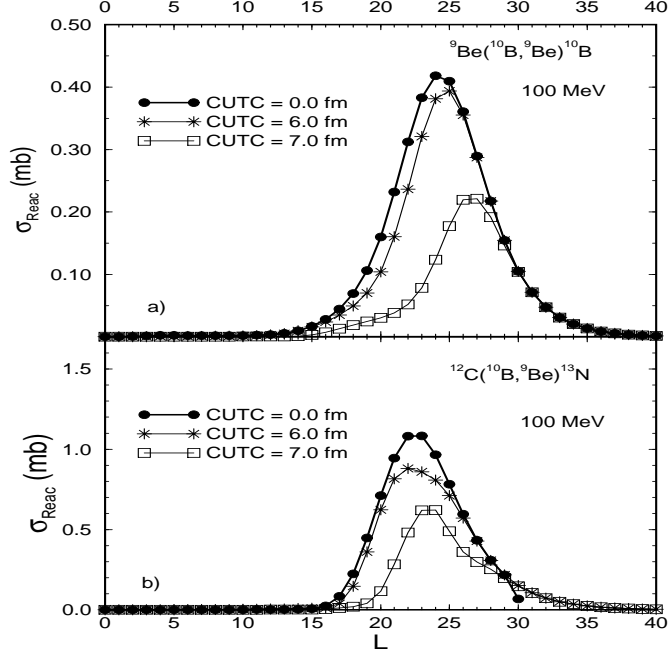


FIG. 9. Calculated reaction cross section for each partial wave L , for ${}^9\text{Be}({}^{10}\text{B}, {}^9\text{Be}){}^{10}\text{B}$ and ${}^{12}\text{C}({}^{10}\text{B}, {}^9\text{Be}){}^{13}\text{N}$ at $E_{\text{lab}} = 100$ MeV.

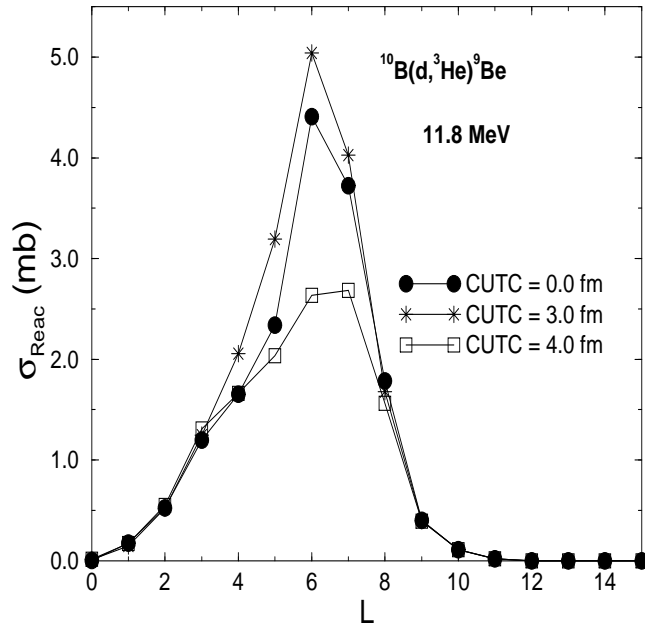


FIG. 10. Calculated reaction cross section for each partial wave L , for ${}^{10}\text{B}(\text{d}, {}^3\text{He}){}^9\text{Be}$ at $E_{\text{lab}} = 11.8$ MeV.

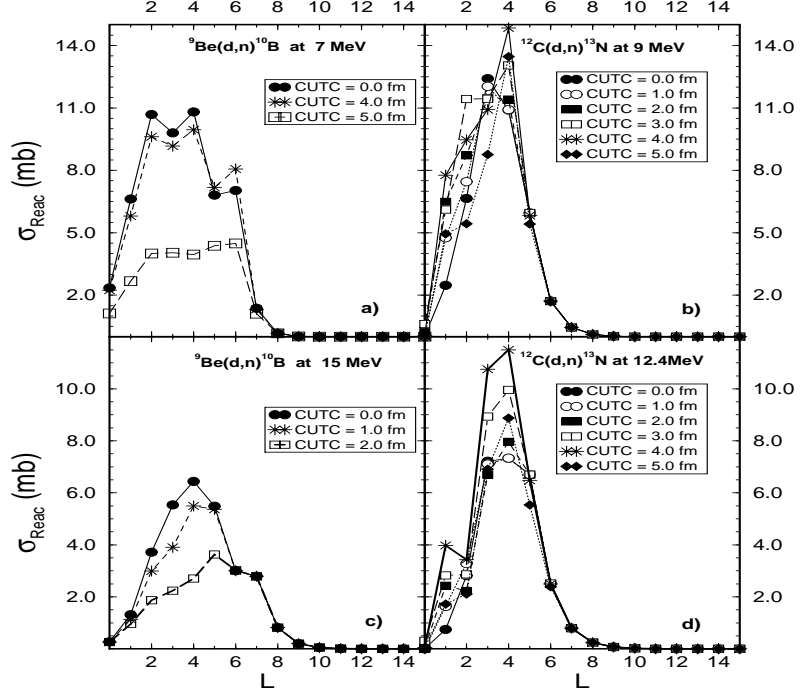


FIG. 11. Calculated reaction cross section for each partial wave L , for ${}^9\text{Be}(\text{d},\text{n}){}^{10}\text{B}$ at 7 and 15 MeV, and ${}^{12}\text{C}(\text{d},\text{n}){}^{13}\text{N}$ reactions at 9 and 12.4 MeV.